

UNCOVERing the contribution of black holes to reionization

Pratika Dayal¹, Marta Volonteri², Jenny E. Greene³, Vasily Kokorev¹, Andy D. Goulding³, Christina C. Williams⁴, Lukas J. Furtak⁵, Adi Zitrin⁵, Hakim Atek⁶, Rachel Bezanson⁷, Iryna Chemerynska⁶, Robert Feldmann⁸, Karl Glazebrook⁹, Ivo Labbe⁹, Themiya Nanayakkara⁹, Pascal A. Oesch^{10, 11}, and John R. Weaver¹²

¹ Kapteyn Astronomical Institute, University of Groningen, PO Box 800, 9700 AV Groningen, The Netherlands
e-mail: p.dayal@rug.nl

² Institut d'Astrophysique de Paris, CNRS, Sorbonne Université, 98bis Boulevard Arago, 75014, Paris, France

³ Department of Astrophysical Sciences, Princeton University, 4 Ivy Lane, Princeton, NJ 08544, USA

⁴ NSF's National Optical-Infrared Astronomy Research Laboratory, 950 North Cherry Avenue, Tucson, AZ 85719, USA

⁵ Physics Department, Ben-Gurion University of the Negev, P.O. Box 653, Be'er-Sheva 84105, Israel

⁶ Institut d'Astrophysique de Paris, CNRS, Sorbonne Université, 98bis Boulevard Arago, 75014, Paris, France

⁷ Department of Physics & Astronomy and PITT PACC, University of Pittsburgh, Pittsburgh, PA 15260, USA

⁸ Department of Astrophysics, University of Zurich, Winterthurerstrasse 190, 8057 Zurich, Switzerland

⁹ Centre for Astrophysics and Supercomputing, Swinburne University of Technology, PO Box 218, Hawthorn, VIC 3122, Australia

¹⁰ Department of Astronomy, University of Geneva, Chemin Pegasi 51, 1290 Versoix, Switzerland

¹¹ Cosmic Dawn Center (DAWN), Niels Bohr Institute, University of Copenhagen, Jagtvej 128, København N, DK-2200, Denmark

¹² Department of Astronomy, University of Massachusetts Amherst, Amherst MA 01003, USA

February 24, 2025

ABSTRACT

Context. With its sensitivity in the rest-frame optical, the James Webb Space Telescope (JWST) has uncovered active galactic nuclei (AGN), comprising both intrinsically faint and heavily reddened sources, well into the first billion years of the Universe, at $z \sim 4 - 11$.

Aims. In this work, we revisit the AGN contribution to reionization given the high number densities associated with these objects.

Methods. We use the DELPHI semi-analytic model, base-lined against the latest high-redshift datasets from the JWST and the Atacama Large millimetre Array (ALMA) to model early star forming galaxies and AGN. We calculate the escape fractions of ionizing radiation from both star formation and AGN and include the impact of reionization feedback in suppressing the baryonic content of low-mass galaxies in ionized regions. This model is validated against the key observables for star forming galaxy, AGN and reionization.

Results. In our *fiducial* model, reionization reaches its mid-point at $z \sim 6.9$ and ends by $z \sim 5.9$. Low stellar mass ($M_* \lesssim 10^9 M_\odot$) star forming galaxies are found to be the key drivers of the reionization process, providing about 77% of the total photon budget. Despite their high numbers, high accretion rates and higher escape fractions compared to star forming galaxies at $z \sim 5$, AGN only provide about 23% of the total reionization budget which is dominated by black holes in high stellar mass systems (with $M_* \gtrsim 10^9 M_\odot$). This is because AGN number densities become relevant only at $z \lesssim 7$ - as a result, AGN contribute as much as galaxies as late as $z \sim 6.2$, when reionization is already in its end stages. Finally, we find that even contrasting models of the AGN ionizing photon escape fraction (increasing or decreasing with stellar mass) do not qualitatively change our results.

Key words. cosmology: reionization – galaxies: high-redshift – ISM: dust – galaxies: quasars: supermassive black holes – cosmology: theory

1. Introduction

The progress of reionization and its key sources remain outstanding questions in the field of physical cosmology. This is because the process of reionization depends on a number of poorly understood quantities including the abundance of galaxies in the first billion years, their star formation/black hole accretion rates that determine the production rate of ionizing photons, the fraction of such photons that can escape out of the galactic environment into the intergalactic medium (IGM) and the (spatially- and temporally-varying) clumping factor of the IGM that determines the recombination rate, to name a few (for reviews see e.g. Dayal & Ferrara 2018; Robertson 2022).

Consensus has been growing that low-mass galaxies are the most probable drivers of the reionization process, given their number densities that show a rising trend down to absolute mag-

nitudes as faint as $M_{UV} \sim -15$ (e.g. Robertson et al. 2015; Madau 2017; Dayal et al. 2020; Trebitsch et al. 2022; Atek et al. 2024; Rinaldi et al. 2023). Black holes seem to contribute at most a few tens of percent to the reionization process, mostly in its end stages at $z \lesssim 5$ (e.g. Onoue et al. 2017; Dayal et al. 2020; Trebitsch et al. 2023). However, such results crucially depend on the number density of active galactic nuclei (AGN), especially in intermediate-mass halos (given that black hole accretion can produce 10 times as many ionizing photons as star formation per unit baryon) in addition to the escape fraction of ionizing photons from such sources (e.g. Dayal et al. 2020). Before the advent of the James Webb Space Telescope (JWST), a number of observations (e.g. Giallongo et al. 2015; Boutsia et al. 2018; Giallongo et al. 2019; Fujimoto et al. 2022) had already hinted at a larger than expected number density of faint AGN at $z > 4$ although such results remained highly debated (McGreer et al.

2018; Parsa et al. 2018; Akiyama et al. 2018). The proposal was that such number densities holding up to higher redshifts might imply a significant AGN contribution to the reionization process (e.g. Grazian et al. 2018; Mitra et al. 2018). Overall, the relative importance of star forming galaxies and AGN to reionization has remained a key outstanding issue, mostly driven by a lack of statistically significant samples of black holes at $z \gtrsim 6$.

With its sensitivity, recent observations with the JWST have been crucial in shedding light on the AGN population at $z \gtrsim 4$: firstly, the detection of broadened Hydrogen Alpha ($H\alpha$) lines from deep JWST spectroscopy have been used to detect the ubiquitous presence of intrinsically faint AGN at $z \gtrsim 4$ (Harikane et al. 2023b; Maiolino et al. 2024b,a). Secondly, the JWST has yielded a new population of intrinsically bright, reddened sources, “little red dots” (LRDs), that exhibit extremely small sizes (of the order of a few hundred parsecs) and a characteristic “V-shaped” continuum which is red in the rest-frame optical but has a blue slope in the rest-frame ultra-violet (UV; Labbé et al. 2023b,a; Furtak et al. 2023). Spectroscopic follow-ups of these sources reveal clearly broadened Balmer lines which have been used to infer the presence of accreting black holes (e.g. Furtak et al. 2024; Kokorev et al. 2023; Fujimoto et al. 2024; Greene et al. 2024; Matthee et al. 2024; Kocevski et al. 2023; Übler et al. 2023; Kokorev et al. 2024). Whilst accounting for a few percent of the galaxy population at $z > 5$, these relatively faint AGN seem to account for about 10–20% of broad-line selected AGN at $z \sim 5–6$ (Harikane et al. 2024; Maiolino et al. 2024a). These combined observations have been used to infer black hole masses ranging between $10^{6.5–8} M_\odot$ (Harikane et al. 2024; Maiolino et al. 2024b,a; Kocevski et al. 2023; Furtak et al. 2024; Larson et al. 2023; Bogdán et al. 2024; Goulding et al. 2023; Kokorev et al. 2023, 2024).

In this work, we revisit the black hole contribution to reionization in light of these newly-detected AGN well within the first billion years. In addition to new modes of black hole seeding and growth required to match to JWST observations, this model – termed DELPHI-DUSTBH includes all of the relevant dust processes and has been base-lined against the latest dust observations from the Atacama Large millimetre Array (ALMA) surveys at $z \sim 5–7$ (Béthermin et al. 2020; Bouwens et al. 2022). This is particularly crucial given that observationally, the escape fractions of ionizing photons from star forming sources is closely linked to their dust enrichment (e.g. Chisholm et al. 2022). We start by describing the semi-analytic model used for this analysis in Sec. 2, the escape fractions of ionizing photons from star forming galaxies and AGN in Sec. 2.1 and the reionization-feedback weighted emissivity in Sec. 2.2. We then validate the model by showing its comparison to the ultra-violet luminosity function (UV LF) in Sec. 3.1 before discussing the emissivity and escape fractions from galaxies and AGN in Sec. 3.2. We validate the model in Sec. 3.3, detail the contribution of galaxies and AGN to reionization in Sec. 3.4 and explore the cumulative AGN contribution for two different models of black hole escape fractions in Sec. 3.5 before concluding in Sec. 4.

We adopt a Λ CDM model with dark energy, dark matter and baryonic densities in units of the critical density as $\Omega_\Lambda = 0.673$, $\Omega_m = 0.315$ and $\Omega_b = 0.049$, respectively, a Hubble constant $H_0 = 100 h \text{ km s}^{-1} \text{ Mpc}^{-1}$ with $h = 0.673$, spectral index $n = 0.96$ and normalisation $\sigma_8 = 0.81$ (Planck Collaboration et al. 2020). Throughout this work, we use a Salpeter initial mass function (IMF; Salpeter 1955) between $0.1–100 M_\odot$. Finally, we quote all quantities in comoving units, unless stated otherwise, and express all magnitudes in the standard AB system (Oke & Gunn 1983).

2. The Theoretical model

This work is based on using the DELPHI (Dark Matter and the emergence of galaxies in the epoch of reionization) semi-analytic model for galaxy formation that uses a binary merger tree approach to jointly track the build-up of dark matter halos, their baryonic components (gas, stellar, dust and metal masses) and black holes. This version, that tracks the seeding and assembly of black holes driven by recent JWST observations, and the dust enrichment of early sources motivated by ALMA results, is termed DELPHI-DUSTBH. It follows the assembly of dark matter halos between $\log(M_h/M_\odot) = 8–14$ from $z \sim 40$ down to $z = 4.5$ in time-steps of 30 Myrs. At any time-step, the available gas mass (from both mergers and accretion) can form stars with an “effective” star formation efficiency which is the minimum between the efficiency that produces enough type II Supernova (SNII) energy to eject the remainder of the gas and an upper maximum threshold (f_*). The two free parameters concerning star formation are $f_* \sim 10\%$ and the fraction of SNII energy that can couple to gas ($f_w \sim 7.5\%$). Their values are obtained by simultaneously matching to the faint and bright-ends of the Lyman Break Galaxy (LBG) UV LF at $z \sim 5–9$, and to the dust-stellar mass relations obtained from the latest ALMA observations (Béthermin et al. 2020; Bouwens et al. 2022). The (about 5 times higher) value of f_* here compared to our previous model DELPHI2019 (Dayal et al. 2019) is driven by dust attenuation which plays a specially crucial role for high-mass systems. In this case, we require a higher star formation efficiency to match to the observed bright-end of the UV LF (for details see Dayal et al. 2022; Mauerhofer & Dayal 2023). Further, every newly formed stellar population (i.e. newly formed stellar mass within a given time-step) is assumed to have an age of 2 Myrs. This age is used in conjunction with its metallicity, that is tracked by our model, to calculate the ionizing photon production rate using the STARBURST99 (Leitherer et al. 1999) stellar population synthesis code.

Further, while the details of black hole physics (growth from both accretion and instantaneous mergers and the associated feedback and a radiative efficiency of $\epsilon_r = 10\%$) remain the same as in our previous works (Dayal et al. 2019, 2020), we now summarise the key new ingredients required to match to the AGN populations being observed by the JWST:

1. Explaining the black hole masses inferred for a number of observed early black holes requires black hole seeds heavier than those from Population III stars which have masses of the order of $\sim 150 M_\odot$ (as discussed in e.g. Kokorev et al. 2023; Furtak et al. 2024; Maiolino et al. 2024a; Natarajan et al. 2024) as used in our previous works (Dayal et al. 2019). We therefore seed the starting halos of any merger tree at $z \gtrsim 13$ with heavy seeds of masses (randomly chosen) between $10^{3–5} M_\odot$. Widespread seeds with masses $\sim 10^3 M_\odot$ can form in dense, massive stellar clusters through a number of pathways (for a review see Sec. 2.3.1 Amaro-Seoane et al. 2023) including dynamical interactions (e.g. Devecchi & Volonteri 2009), the runaway merger of stellar mass black holes (e.g. Belczynski et al. 2002) or the growth of stellar mass black holes in conjunction with mergers (e.g. Leigh et al. 2013). They can grow to larger masses within the clusters (Alexander & Natarajan 2014). Additionally, seeds with masses at birth up to $10^5 M_\odot$ can form via supermassive star formation, sometimes referred to as direct collapse black holes, although this mechanism produces a lower number of viable seeds (Dayal et al. 2019).
2. Our model includes a “critical” halo mass for efficient black hole accretion with a value that evolves with redshift as

Table 1: Free parameters (column 1), their symbols (column 2), the values used in the pre-JWST version of the DELPHI model (DELPHI2019, DAYAL ET AL. 2019) in column 3 and the values used in this work (DELPHI-DUSTBH; column 4) that have been calibrated against datasets from both ALMA and the JWST. These differences and their physical implications are discussed in Sec. 2.

Parameter	Symbol	DELPHI2019	DELPHI-DUSTBH
Maximum star formation efficiency	f_*	0.02	0.1
Fraction of SNII energy coupling to gas	f_w	0.1	0.075
BH seed mass	-	$150M_\odot$	$10^{3-5}M_\odot$
Radiative efficiency of black hole accretion	ϵ_r	0.1	0.1
Fraction of AGN energy coupling to gas	f_{bh}^w	0.003	0.001
Fraction of gas mass AGN can accrete	$f_{bh}^{ac}(M_h < M_h^{crit})$	5.5×10^{-4}	5.5×10^{-4}
Fraction of gas mass AGN can accrete	$f_{bh}^{ac}(M_h > M_h^{crit})$	5.5×10^{-4}	0.1
Fraction of Eddington rate for BH accretion	$f_{Edd}(M_h < M_h^{crit})$	7.5×10^{-5}	10^{-4}
Fraction of Eddington rate for BH accretion	$f_{Edd}(M_h \geq M_h^{crit})$	1	1
Escape fraction of H I ionizing photons from star formation	f_{esc}^{sf}	$0.02[(1+z)/7]^{2.8}$	$f_{esc}^{sf} = \text{fn}(\beta)^\dagger$
Escape fraction of H I ionizing photons from AGN	f_{esc}^{bh}	Ueda et al. (2014)	$f_{esc}^{bh} = \text{fn}(f_{Edd})^\ddagger$
Stellar population synthesis model	-	STARBURST99	STARBURST99
Reionization (UVB) feedback	-	No	Yes

Notes. [†] As detailed in Sec. 2.1, the value of f_{esc}^{sf} is determined using observed relations (Chisholm et al. 2022) that link f_{esc}^{sf} to the UV spectral slope (β).

[‡] Further, f_{esc}^{bh} is inferred from the Eddington accretion fraction (f_{Edd}) based on the results of zoom-in hydrodynamic simulations (Trebitsch et al. 2019).

$M_{bh}^{crit}(z) = 10^{11.25} [\Omega_m(1+z)^3 + \Omega_\Lambda]^{-0.125}$ on which we include a scatter of 0.5 dex, motivated by the results of cosmological simulations (e.g. Bower et al. 2017). In order to explain the number density of JWST-detected AGN we modify some of the parameters. Black holes are allowed a gas accretion rate of $M_{bh}^{ac}(z) = \min[\epsilon_r f_{bh}^{ac} M_g^{sf}, f_{Edd} M_{Edd}]$ where M_g^{sf} is the gas mass left after star formation and its associated SNII feedback, f_{Edd} is the Eddington fraction and M_{Edd} is the Eddington accretion rate. Allowing very weak AGN feedback (0.01% of black hole feedback coupling to the gas) we require values of $f_{bh}^{ac} = 0.1$ (5×10^{-4}) and $f_{Edd} = 1.0$ (10^{-4}) for halos above (below) the critical mass (we allow 0.5 dex of scatter on all of these quantities). That is, black holes in high-mass (low-mass) halos can accrete the minimum between 10% (0.05%) of the available gas mass and 100% (0.01%) of the Eddington fraction. High-gas accretion rates in halos above the critical halo mass are crucial to simultaneously match to AGN observables including the bolometric and UV LFs, and black hole mass functions.

3. We include the impact of dust attenuation on the luminosity and ionizing photon escape fractions for both star formation and AGN, as detailed in Sec. 2.1.
4. Finally, we account for a coupling of reionization feedback and galaxy formation in order to determine the role of star formation and AGN in the reionization process as detailed in Sec. 2.2.

2.1. Dust and the escape fraction of ionizing photons

The escape fraction of ionizing photons from star forming galaxies and AGN remain a key outstanding issue in the field of reionization (e.g. Sec. 7.1, Dayal & Ferrara 2018). In this work, we use simple phenomenological prescriptions to obtain the escape fraction from star formation (f_{esc}^{sf}) and AGN (f_{esc}^{bh}). For star forming galaxies (as in our previous work, Trebitsch et al. 2022), we use the results from the Low- z Lyman Continuum survey (LzLCS Flury et al. 2022) that targets 66 $z \sim 0.3$ Lyman continuum emitters which can be treated as analogues of early sources. For this

sample, f_{esc}^{sf} is closely linked to the UV spectral slope (β) between 1300-1800Å as characterised in Chisholm et al. (2022):

$$f_{esc}^{sf} = (1.3 \pm 0.6) \times 10^{-4} \times 10^{(-1.22 \pm 0.1)\beta} \quad (1)$$

Further, high- z observations (e.g. Bouwens et al. 2014) show a correlation between the β slope and the observed (dust attenuated) UV magnitude such that (see e.g. Trebitsch et al. 2022)

$$\beta = -1.993 - 0.071(z - 6) - 0.125(M_{UV} + 19.5). \quad (2)$$

The above relations imply an increase in f_{esc}^{sf} with a decrease in dust attenuation i.e. with bluer β slopes. We calculate the dust attenuated magnitude for star forming galaxies using the model detailed in Dayal et al. (2022). Essentially, we use the latest metal yields from Kobayashi et al. (2020) and calculate the dust mass including the key processes of dust formation, destruction, ejection, astration and grain growth in the interstellar medium (ISM); we assume a grain growth timescale of 30 Myr timescale. This has been shown to yield results in accord with the latest ALMA observations for $z \gtrsim 5$ galaxies (Dayal et al. 2022; Mauerhofer & Dayal 2023). This dust is assumed to be perfectly mixed with the gas in order to calculate the optical depth to UV photons to obtain the dust-attenuated UV magnitude.

As for the dust attenuation of black holes, we use results from zoom-in simulations that estimate the column density of gas around black holes in high-redshift galaxies (Trebtsch et al. 2019). These simulations find that gas density in the central region of galaxies (~ 40 pc), which dominates the total column density from the AGN to the galaxy edge, is modulated by inflows and outflows, leading to a scaling of the form:

$$\frac{N_H}{10^{22} \text{cm}^{-2}} = \left(\frac{f_{Edd}}{0.01} \right)^{0.5}. \quad (3)$$

Note that this does not include an explicit “torus”. However, given the high gas content in high- z galaxies the ISM column density is a significant, if not dominant, component (see Circosta et al.

2019). Assuming a 0.5 dex of scatter on this relation, the inferred column density can be used to calculate the UV optical depth as $\tau_{bh}(\lambda) = \int n_d \sigma_d(\lambda) dl$ where n_d is the number density of dust grains and σ_d is the dust interaction cross-section per unit hydrogen atom using the fits from Gnedin et al. (2008) based on the Small Magellanic Cloud (SMC) model. Further, given that we only model the total gas, dust and metal masses in our model, we assume the dust number density to be $n_d = n_g (Z/Z_\odot)$ where n_g is the number density of gas particles and Z is the gas phase metallicity normalised to the mean SMC metallicity of $Z_\odot = 0.005$. We then assume the same escape fraction for UV and ionizing photons from AGN such that $f_{esc}^{bh} = e^{-\tau_{bh}}$.

2.2. The progress of reionization and its impact on galaxy formation

We can now calculate the volume filling fraction of ionized hydrogen (Q_{II}) to track the progress of reionization as (Shapiro & Giroux 1987; Madau et al. 1999; Dayal et al. 2020):

$$\frac{dQ_{II}}{dz} = \frac{dn_{ion}}{dz} \frac{1}{n_H} - \frac{Q_{II}}{t_{rec}} \frac{dt}{dz}. \quad (4)$$

Here, $\dot{n}_{ion} = dn_{ion}/dz$ is the total escaping rate of ionizing photons (from both star formation and AGN), n_H is the co-moving hydrogen number density and t_{rec} is the recombination timescale for ionized hydrogen - we use an IGM clumping factor of $C = 1 + 43 z^{-1.71}$ (Pawlik et al. 2009) to calculate t_{rec} (for complete details see Dayal et al. 2020).

The build-up of the heating UV background (UVB) from reionization can suppress the baryonic content of low-mass halos in ionized regions (e.g. Gnedin 2000; Sobacchi & Mesinger 2013; Hutter et al. 2021). We account for this process by running a “maximal UVB” scenario where we completely suppress the gas mass (and the associated star formation and black hole accretion rate) for halos with virial velocities below 50 Km s^{-1} ; this corresponds to halo masses of $10^{9.7} (10^{9.3}) M_\odot$ at $z \sim 5$ (10). The total emerging ionizing emissivity for reionization is then obtained by weighing over the UV-suppressed contribution from low-mass halos in ionized regions (Q_{II}) as well as that from un-suppressed sources in neutral regions ($Q_I = 1 - Q_{II}$) such that (Choudhury & Dayal 2019)

$$\begin{aligned} \dot{n}_{ion}(z) = & f_{esc}^{sf} [Q_{II}(z) \dot{n}_{int,II}^{sf}(z) + Q_I(z) \dot{n}_{int,I}^{sf}(z)] \\ & + f_{esc}^{bh} [Q_{II}(z) \dot{n}_{int,II}^{bh}(z) + Q_I(z) \dot{n}_{int,I}^{bh}(z)], \end{aligned} \quad (5)$$

where the first and second terms on the right hand-side account for the contribution of star forming galaxies and AGN, respectively. As might be expected, while un-suppressed halos dominate at the start of the reionization process, the importance of the UV-suppressed term increases as reionization proceeds. This is the *fiducial* model that is used throughout the paper.

3. Early black holes and the reionization process in light of JWST data

We now validate our model against the UV LF for both star forming galaxies and AGN in Sec. 3.1 before discussing their associated ionizing emissivities and escape fractions in Sec. 3.2. We validate the model against key reionization observables in Sec. 3.3 and discuss the key reionization sources in Sec. 3.4 before ending by showing the AGN contribution for two contrasting models of f_{esc}^{bh} in Sec. 3.5.

3.1. The UV LF for star forming galaxies and AGN

We start by discussing the dust-attenuated UV LF from star forming galaxies, AGN and the total UV luminosity (summed over both these components) as shown in Fig. 1. As noted, our choice of the model parameters for star formation (maximal threshold star formation efficiency and the fraction of SN energy coupling to gas) and dust (consistent with our previous works, e.g. Dayal et al. 2022) are tuned to match to the observed UV LF for LBGs at $z \sim 5-9$ and for AGN at $z \sim 5-7$ in addition to the stellar and black hole mass functions and the AGN bolometric LF. Therefore, by construction, the model yields a dust-attenuated LBG UV LF that is in good agreement with the observations (including those from the JWST), within error bars, for $M_{UV} \sim -16$ to -23.5 at $z \sim 5-7$. This also naturally results in derived quantities such as the UV luminosity density being in accord with observations (for complete details see e.g. Dayal et al. 2022; Mauerhofer & Dayal 2023).

As seen from the same figure, our model for AGN dust attenuation yields an evolving UV LF that is in good accord with JWST observations of both LRDs and faint AGN (with $M_{UV} \sim -18$ to -21.5) at $z \sim 5$ (Matthee et al. 2024; Maiolino et al. 2024b,a; Harikane et al. 2024) and the UV LF at $z \sim 5-7$ from Greene et al. (2024); our results are also in accord with earlier AGN UV LF estimates (e.g. Giallongo et al. 2015; Parsa et al. 2018). However, the model over-predicts the AGN UV LF between $M_{UV} \sim -23$ to -24 as compared to the observations from Niida et al. (2020). This is possibly due to the combination of a simple model for dust attenuation, a mass-independent black hole accretion rate and an up-scattering of low-mass black holes into these high luminosity bins due to the scatter of 0.5 dex assumed on all of the model parameters. A further possibility is that pre-JWST observations may underestimate the bright end of the AGN UV LF. The UV luminosity functions are generally based on spectroscopically confirmed sources from photometric selected samples, and thus may suffer from some incompleteness. It is also important to keep in mind that in some cases, the AGN signatures are detected in the rest-frame optical, and we have incomplete knowledge of the origin of the UV emission which may therefore have a significant contribution from the stellar component. In the case of the little red dots we still do not know the origin of the UV (e.g. Labbé et al. 2023a; Furtak et al. 2023; Greene et al. 2024). Finally, for the X-ray selected sources without spectroscopic follow-up, we do not know the unobscured/obscured fractions (e.g. Giallongo et al. 2015; Parsa et al. 2018).

We find star formation to dominate the faint-to-intermediate end ($M_{UV} \gtrsim -21.5$) of the deconstructed UV LF at $z \sim 5$ with AGN dominating at brighter luminosities (see also Ono et al. 2018; Piana et al. 2022). We find UV faint AGN to contribute $\sim 0.4-15\%$ to the total number density at intermediate luminosities ($M_{UV} \sim -18$ to -21) at this redshift. By $z \sim 7$, AGN dominate the UV LF at much brighter luminosities corresponding to $M_{UV} \sim -23$ - this is naturally expected as both the number densities and masses of massive black holes build up with time. As seen, we find that the intrinsic (dust-unattenuated) AGN UV LF severely over-estimates the bright end of the AGN UV LF; an increasing impact of dust attenuation with decreasing redshift is crucial to match the AGN UV LF to observations.

The stellar component dominates the UV at all magnitudes at $z \sim 10$ where massive black holes have not yet been able to assemble in significant numbers. Indeed at $z \sim 10$, the AGN UV LF predicted by the model is a factor 15-40 lower in the case the number densities of AGN inferred from UHZ1 and GN-z11 correctly represent the AGN population at this redshift (Fujimoto

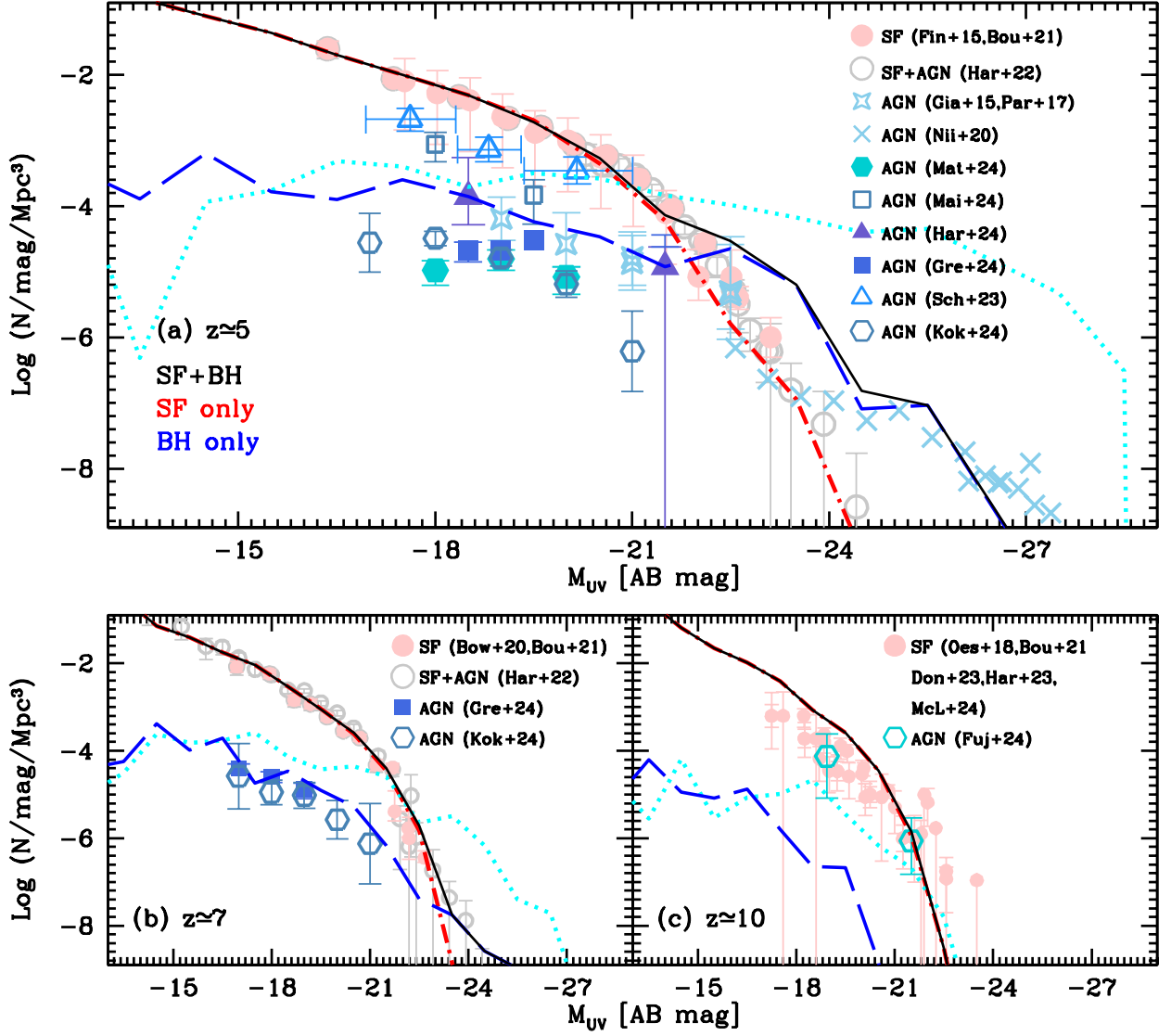


Fig. 1: The rest-frame UV LF at $z \sim 5, 7$ and 10 , as marked. In each panel, the long-dashed, dot-dashed and solid lines show the dust obscured UV LF for AGN, star formation and the “total” luminosity, as marked; dotted cyan lines show the intrinsic (i.e. dust-unattenuated) AGN UV LF. In all panels, points show observational results as marked: at $z \sim 5$ (panel a), for star forming galaxies (solid circles, Finkelstein et al. 2015; Bouwens et al. 2021), galaxies+AGN (empty circles, Harikane et al. 2022), AGN (empty stars and crosses, Giallongo et al. 2015; Parsa et al. 2018; Niida et al. 2020) and the new JWST AGN results from Matthee et al. (2024, filled hexagons), Maiolino et al. (2024b, empty squares), Harikane et al. (2024, filled triangles), Scholtz et al. (2023, empty triangles), Greene et al. (2024, filled squares) and Kokorev et al. (2024, empty hexagons). At $z \sim 7$ (panel b), we show the results for star forming galaxies (solid circles, Bowler et al. 2020; Bouwens et al. 2021), galaxies+AGN (empty circles, Harikane et al. 2022) and the new JWST AGN results from Greene et al. (2024, filled squares) and Kokorev et al. (2024, empty hexagons). At $z \sim 10$ (panel c), we show the UV LF inferred for star forming galaxies (solid circles, Oesch et al. 2018; Bouwens et al. 2021; Donnan et al. 2023; Harikane et al. 2023a; McLeod et al. 2024). At this redshift, the empty hexagons show AGN candidates (UHZ1 and GN-z11) with the number densities calculated as detailed in Fujimoto et al. (2024).

et al. 2024). We however caution that the nature of these two sources is poorly known. Indeed, it is highly plausible that the observed UV luminosity has a significant contribution from star formation rather than being powered by AGN accretion alone. Within error bars, these observed number densities are in accord with the “intrinsic” (i.e. dust-unattenuated) AGN UV LF from our model. Accounting for these objects and assuming an upper limit of $f_{\text{esc}}^{\text{bh}} = 1$ would yield the maximum AGN contribution to reionization. The results of this model are discussed in Sec. 3.4 where we show that such a model can be ruled out since it severely overshoots the observed emissivity constraints at $z \lesssim 6$.

3.2. The ionizing emissivity and its escape fraction from star formation and black holes

We now discuss the intrinsic production rate of ionizing photons as a function of stellar mass from both star forming galaxies ($\dot{n}_{\text{int}}^{\text{sf}}$) and AGN ($\dot{n}_{\text{int}}^{\text{bh}}$) at $z \sim 5 - 10$, as shown in (panel a of) Fig. 2. We find that $\dot{n}_{\text{int}}^{\text{sf}}$ scales with M_* at all $z \sim 5 - 10$ since in our model, both the stellar mass assembly and the instantaneous star formation rate are closely tied to the underlying halo potential. The mean relation for star formation can be described by $\dot{n}_{\text{int}}^{\text{sf}} = 0.9M_* + \delta$ where $\delta = (45.9, 46.3, 46.6)$ at $z \sim (5, 7, 10)$,

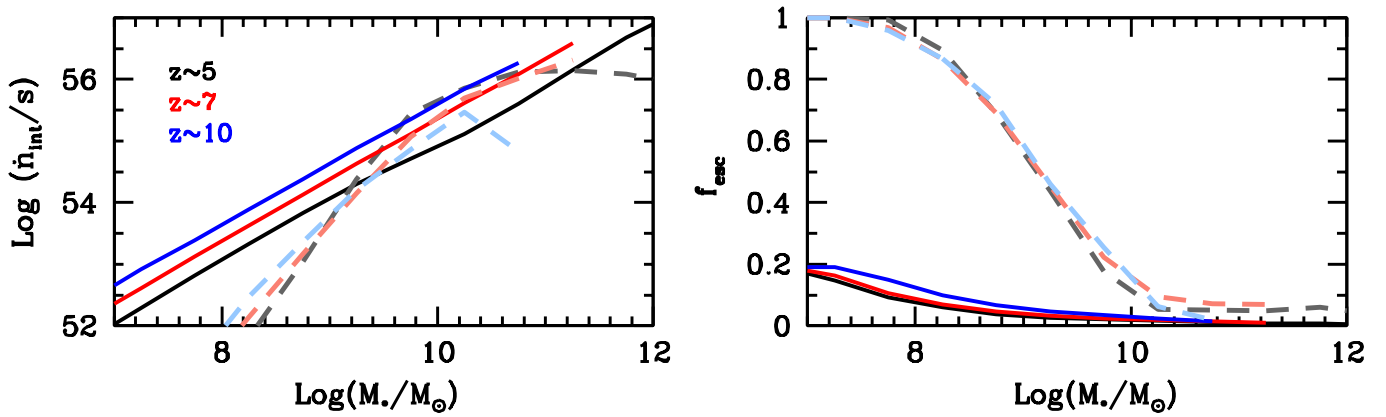


Fig. 2: As a function of the stellar mass, we show the intrinsic production rate of ionizing photons (*left panel*) and their escape fractions (*right panel*) at $z \sim 5 - 10$, as marked. In each panel, the solid and dashed lines show the results for star formation and black holes, respectively.

respectively. The amplitude of the relation increases with redshift because galaxies of a given stellar mass are hosted in halos of similar masses at all $z \sim 5 - 10$. However, halos of a given mass correspond to deeper potentials with increasing redshift which result in an increase in the star formation rate and therefore an increase in the production rate of ionizing photons. The behaviour of AGN is more mass-dependent (see e.g. Dayal et al. 2020): for example, at $z \sim 5$, $\dot{n}_{\text{int}}^{\text{bh}}$ essentially scales with the stellar mass for $M_* \sim 10^8 - 10^{10} M_\odot$ galaxies, thereafter flattening out to $M_* \sim 10^{12} M_\odot$ - this is driven by the fact that although high mass galaxies have an availability of gas, the black hole can only accrete the minimum between 10% of the gas mass and 100% of the Eddington limit as discussed in Sec. 2. At $z \sim 5$, $\dot{n}_{\text{int}}^{\text{bh}}$ exceeds $\dot{n}_{\text{int}}^{\text{sf}}$ for $M_* \gtrsim 10^{9.2-11.4} M_\odot$ galaxies. Indeed, for $M_* \sim 10^{10} M_\odot$ systems, black holes produce about 5 times as many ionizing photons ($\dot{n}_{\text{int}}^{\text{bh}} \sim 10^{55.8} \text{s}^{-1}$) as star formation. The same qualitative behaviour persists at $z \sim 7$ where black holes contribute roughly equally as star formation to the ionizing photon production rate for $M_* \sim 10^{10-11} M_\odot$ galaxies which is of the order of $\dot{n}_{\text{int}}^{\text{bh}} \sim 10^{55-56} \text{s}^{-1}$. At $z \sim 10$, however, massive enough black holes have not had time to assemble, as a result of which the stellar component dominates the ionizing photon production rate for all stellar masses.

We then discuss the trend of the escape fraction of ionizing photons from star formation and AGN as shown in (panel b) of the same figure. Given its direct dependence on the dust mass that increases with M_* , $f_{\text{esc}}^{\text{sf}}$ too decreases with an increase in the stellar mass. For example, at $z \sim 5$ $f_{\text{esc}}^{\text{sf}}$ decreases from about 16% for $M_* \sim 10^7 M_\odot$ to $\sim 0.6\%$ for $M_* \sim 10^{12} M_\odot$. For a given stellar mass, the slight decrease in the dust attenuation with increasing redshift results in a mild increase of $f_{\text{esc}}^{\text{sf}}$ with z - for example, $f_{\text{esc}}^{\text{sf}}$ increases from 2.5% to 5% for $M_* \sim 10^9 M_\odot$ between $z \sim 5$ and 10. As for AGN, black holes in galaxies with $M_* \lesssim 10^{8.5} M_\odot$ show $f_{\text{esc}}^{\text{bh}} \gtrsim 80\%$ given their low Eddington accretion rates. We find $f_{\text{esc}}^{\text{bh}}$ to show a steep drop for more massive systems due to an increase in both the Eddington accretion rate and metallicity which drive up the dust optical depth. For example, by $M_* \sim 10^{10} M_\odot$, $f_{\text{esc}}^{\text{bh}}$ drops to about 15% at $z \sim 5 - 7$. We caution that this simple phenomenological model assumes spherical symmetry in calculating the escape fraction of ionizing photons from both star formation and AGN - in principle, however, there might be (dusty) dust-free lines of sight that would result in much (lower) higher escape fractions.

3.3. Validating the model against reionization observables

We now validate the model results against the two key reionization observables - the electron scattering optical depth (τ_{es}) and Q_{II} - whose results are shown in Fig. 3. The model agreement with the early star forming galaxy population and $f_{\text{esc}}^{\text{sf}}$ values that scale inversely with both stellar mass and redshift result in a τ_{es} value in good agreement with the central value inferred from Planck Collaboration et al. (2020) data as seen from (the left panel of) Fig. 3; this result was expected based on our previous works that have used the DELPHI model for reionization, (Dayal et al. 2020; Trebitsch et al. 2023). Given their larger number densities and higher $f_{\text{esc}}^{\text{sf}}$ values, we find low-mass ($M_* \lesssim 10^9 M_\odot$) star forming galaxies to be the key drivers of the reionization process, with higher mass galaxies having a negligible contribution. We also find that black holes in high-mass galaxies ($M_* \gtrsim 10^9 M_\odot$) dominate the AGN contribution to reionization.

As seen from (the right panel of) the same figure, the contribution from both star formation and AGN result in a redshift evolution of Q_{II} that is in good agreement with a number of observational results within error bars (e.g. Fan et al. 2006; Davies et al. 2018; Yang et al. 2020b; Jung et al. 2020; Lu et al. 2020; Bosman et al. 2022; Gaikwad et al. 2023; Nakane et al. 2024); readers are also referred to (Fontanot et al. 2023) for a tabulated compilation. In this *fiducial* model, reionization reaches its mid-point at $z \sim 6.9$ and is over by $z_{\text{reio}} \sim 5.9$. Low-mass ($M_* \lesssim 10^9 M_\odot$) star forming galaxies are the key drivers of reionization for the bulk of its history (discussed further in Sec. 3.4). Indeed, while a scenario ignoring AGN shows no sensible effect on the progress of reionization down to $z \sim 7$, the end of the process is delayed to $z \sim 5$ (i.e. by about 200 Myrs). In an AGN-only scenario, on the other hand, the redshift evolution of Q_{II} is naturally delayed, with the mid-point of reionization being reached at $z \sim 6$. Driven by an increase in both the number densities and masses of black holes at $z \lesssim 6$, reionization proceeds at an accelerated rate in this scenario and is over by $z \sim 5.2$, driven mostly by AGN in high-mass ($M_* \gtrsim 10^9 M_\odot$) galaxies. An AGN-only scenario can be ruled out because it generates too low a value of $\tau_{\text{es}} = 0.032$ (as compared to the observed value of 0.054) and is in tension with a number of inferred constraints on Q_{II} at $z \gtrsim 7$, as seen from the same figure.

We note that reionization ends at $z \sim 5.9$ in our *fiducial* model, while recent results on the Lyman α transmission in Quasar spectra seem to indicate reionization-related fluctuations

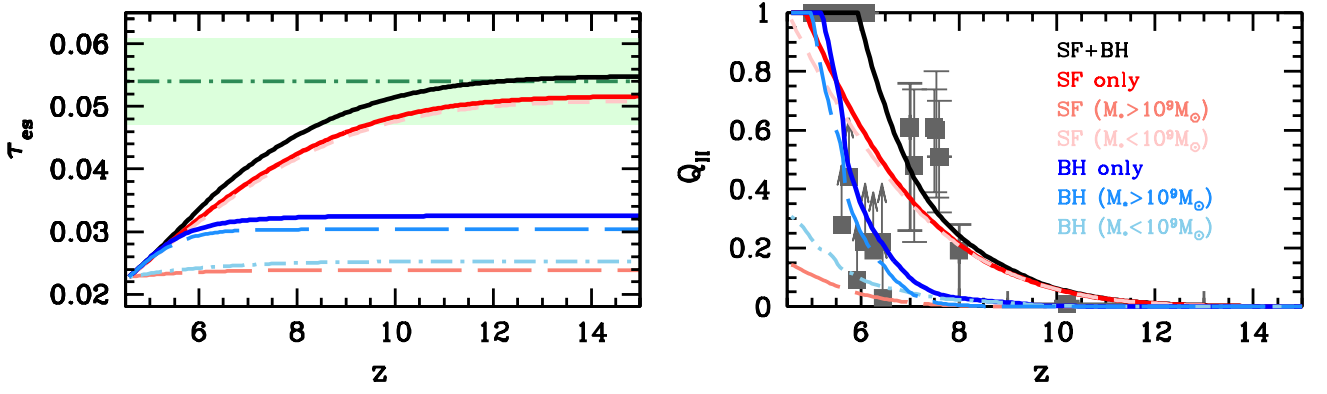


Fig. 3: The redshift evolution of the electron scattering optical depth (*left panel*) and the volume filling fraction of ionized hydrogen (*right panel*). We show the volume filling fraction weighted values from both star forming galaxies and AGN as well as the contribution deconstructed into galaxies with stellar masses above and below $10^9 M_\odot$, as marked. In the left panel, the dot-dashed horizontal line and the shaded region show the electron scattering optical depth and its associated error bars from Planck Collaboration et al. (2020). In the right panel, points show compilations of Q_{II} results from a number of works (Fan et al. 2006; Davies et al. 2018; Yang et al. 2020a; Jung et al. 2020; Lu et al. 2020; Bosman et al. 2022; Gaikwad et al. 2023; Nakane et al. 2024).

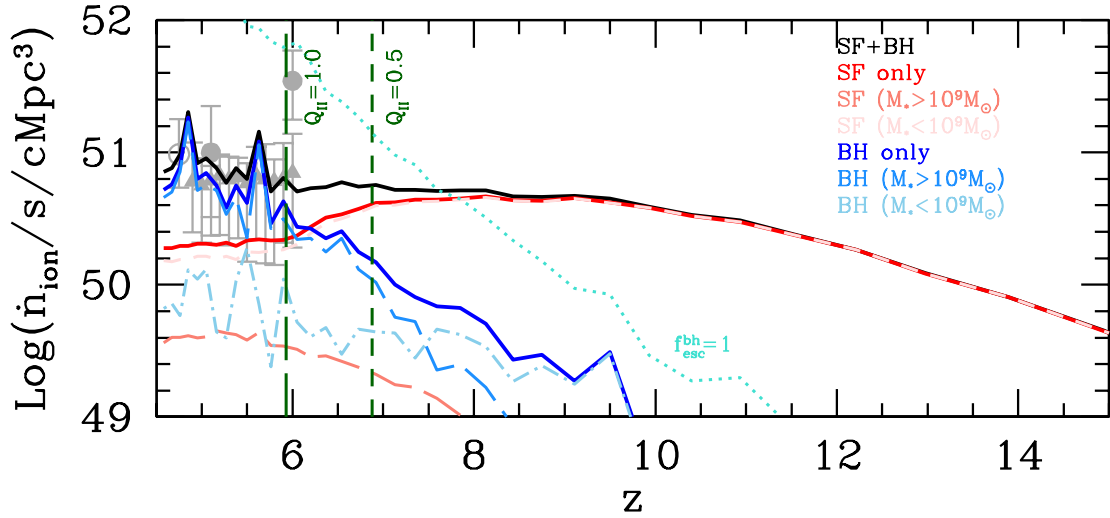


Fig. 4: The redshift evolution of the “escaping” rate of ionizing photons from star forming galaxies and AGN weighted over the volume filling fraction to account for the effects of reionization feedback (Eqn. 5). The dotted line shows the “maximal” AGN contribution assuming $f_{\text{esc}}^{\text{bh}} = 1$. We also show the total contribution deconstructed into sources with stellar masses above and below $10^9 M_\odot$, as marked. Points show the observational results from Becker & Bolton (2013, empty circles), Becker et al. (2021, filled circles) and Gaikwad et al. (2023, filled triangles). The vertical short-dashed (long-dashed) line shows the redshift at which the IGM is half (fully) ionized i.e. $Q_{\text{II}} = 0.5$ (1), as marked.

(in the UVB, residual neutral hydrogen fraction, and/or IGM temperature) to persist in the IGM down to $z \sim 5.3$, signalling a late end to the reionization process (Bosman et al. 2022). This discrepancy could arise from a number of assumptions in our work that could have a significant bearing on the end of reionization as now detailed. Firstly, as detailed in Sec. 2.1, we assign values of $f_{\text{esc}}^{\text{sf}}$ and $f_{\text{esc}}^{\text{bh}}$ based on the dust enrichment of the galaxy and the Eddington fraction, respectively. However, the escape of ionizing radiation is a highly stochastic process that depends on the line-of-sight (e.g. Paardekoooper et al. 2015; Trebitsch et al. 2017) and is strongly modulated over timescales of Myrs due to both Supernova and radiative feedback (e.g. Rosdahl et al. 2022). Secondly, we assume complete suppression of the gas mass for halos in ionized regions below a fixed virial velocity of 50 km s^{-1} . Suppressing the gas content in more (less) massive halos by about 0.5 dex would shift the end stages of reionization

by $\delta z \sim 0.5$ as we have shown in a previous work (Trebitsch et al. 2022). However this would impact both star formation and AGN growth, which would not significantly impact our results on the relative contributions of these sources to the reionization process. Finally, given the nature of the model, we can only track the volume filling fractions of neutral/ionized hydrogen rather than the reionization-related fluctuations measured by observations. We aim at fully implementing our semi-analytic model into a hydrodynamic framework to be able to track these fluctuations at the end stages of reionization in future works.

3.4. The key sources of reionization

We now discuss the relative contribution of star forming galaxies and AGN to the reionization process accounting for its feedback (Eqn. 5) as shown in Fig. 4. As noted above, in our *fiducial*

model, the mid-point of reionization occurs at $z \sim 6.9$ with reionization being over by $z \sim 5.9$. Star formation in low-mass galaxies (with $M_* \lesssim 10^9 M_\odot$) is the key driver of the reionization process, providing $> 80\%$ of ionizing photons at any redshift between $z \sim 7.1 - 20$. As reionization proceeds and the volume filling fraction exceeds 50% at $z \sim 6.9$, the gas masses and star formation rates of such sources are increasingly suppressed by UV feedback. This results in the emissivity from star formation turning over at $z \lesssim 7$ and dropping from providing 75% of ionizing photons at $z \sim 7$ to 33% by the end of reionization at $z \sim 5.9$. With their lower number densities, star formation in high-mass galaxies (with $M_* \gtrsim 10^9 M_\odot$) has a negligible contribution ($\lesssim 5\%$) at any redshift between $z \sim 6 - 20$.

As an increasing number of massive black holes assemble through efficient accretion, the AGN contribution to reionization increases with cosmic time from about 26% at $z \sim 7$ to 66% by $z \sim 5.9$. This contribution is originally driven by putative black holes in low-mass sources ($M_* \lesssim 10^9 M_\odot$) at $z \gtrsim 7.3$. However, as a result of their larger accretion rates (and hence production rate of ionizing photons) and the UV-suppression of low-mass systems, black holes in high-mass galaxies ($M_* \gtrsim 10^9 M_\odot$) start dominating the AGN contribution to reionization at $z \lesssim 7.3$ and make up $\sim 70\%$ of the total AGN budget by $z \sim 6$. However, despite their high numbers, high accretion rates and higher escape fractions (as compared to star formation), AGN only contribute as much as star forming galaxies in terms of the ionizing budget by $z \sim 6.2$ when reionization is already 80% complete and therefore in its end stages.

In terms of the cumulative photon budget in the *fiducial* model, the qualitative picture is very similar. Dominating the photon contribution for most of the reionization history, star formation in low-mass galaxies ($M_* \lesssim 10^9 M_\odot$) provides more than two-thirds ($\sim 77\%$) of the cumulative photon budget; star formation in higher-mass halos play a negligible role, providing $< 3\%$ of the total reionization photon budget. As a result of their rising number densities at $z \lesssim 7$, AGN provide a fourth (about 23%) of the reionization budget - this is mostly driven by AGN in high-mass halos ($M_* \gtrsim 10^9 M_\odot$) which make up about 16.5% of the budget with AGN in lower mass halos providing the final $\sim 6.5\%$ of reionization photons. Our result of star formation in low-mass galaxies being the key reionization driver (e.g. Robertson et al. 2015; Atek et al. 2024), with AGN playing a role only towards the very end stages is in excellent accord with previous works (e.g. Chardin et al. 2017; Onoue et al. 2017; Dayal et al. 2020; Trebitsch et al. 2023).

Finally, we show a “maximal” AGN contribution case in which AGN are assumed to be completely dust-free at $z \gtrsim 7$ i.e. $f_{\text{esc}}^{\text{bh}} = 1$. This model is driven by the tentatively high amplitude of the AGN UV LF inferred at $z \sim 10$, which is in accord with a dust-free AGN scenario, as shown in Sec. 3.1. As seen from Fig. 4, in this case, AGN and galaxies contribute equally to the ionizing photon output by $z \sim 7.5$. However, given the steeply rising AGN contribution reionization finishes as early as $z \sim 7$ in this model. By this point, AGN contribute 36% to the cumulative photon budget. However, as pointed out in our previous works (Dayal et al. 2020, e.g.), we reiterate that this case can be ruled out since it exceeds the emissivity values observed at $z \lesssim 6$ (by e.g. Becker & Bolton 2013; Becker et al. 2021; Gaikwad et al. 2023) in addition to over-estimating the observed AGN UV LF at $z \sim 5, 7$ as shown in Sec. 3.1.

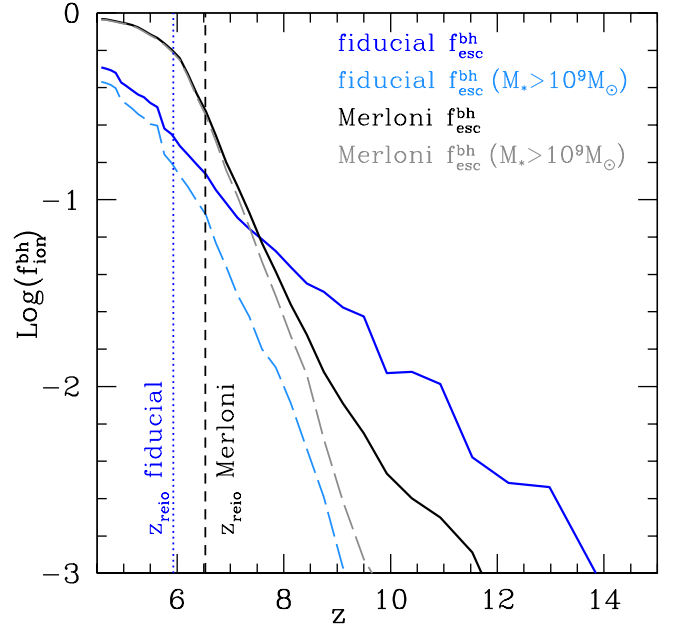


Fig. 5: The cumulative fraction of ionizing photons contributed by AGN as a function of redshift ($f_{\text{ion}}^{\text{bh}}$) as well as the contribution from AGN in high-mass ($M_* \gtrsim 10^9 M_\odot$) galaxies, as marked. We show results for two contrasting models of $f_{\text{esc}}^{\text{bh}}$: the first is the *fiducial* model where $f_{\text{esc}}^{\text{bh}} \propto M_*^{-1}$ and the second is the “Merloni” (Merloni et al. 2014) model where $f_{\text{esc}}^{\text{bh}} \propto M_*$. We also show the redshifts (z_{reio}) at which reionization finishes in both of these models.

3.5. The impact of the escape fraction of ionizing photons from AGN

In order to study the impact of $f_{\text{esc}}^{\text{bh}}$ on our results, we study a contrasting model where we assume that the unobscured fraction of AGN is a proxy for $f_{\text{esc}}^{\text{bh}}$ (see Dayal et al. 2020, for details and extensive comparison of different approaches on $f_{\text{esc}}^{\text{bh}}$). We use the results from Merloni et al. (2014) who find $f_{\text{esc}}^{\text{bh}}$ to scale with the intrinsic X-ray luminosity in the 2-10 keV range in a redshift-independent manner such that

$$f_{\text{esc}}^{\text{bh}} = 1 - 0.56 + \frac{1}{\pi} \arctan\left(\frac{43.89 - \log L_X}{0.46}\right). \quad (6)$$

This model results in a scenario where $f_{\text{esc}}^{\text{bh}} \propto M_*$ such that $f_{\text{esc}}^{\text{bh}}$ increases from 10% to 95% as M_* increases from $10^{9.5}$ to $10^{11} M_\odot$; this is in contrast to the *fiducial* model where $f_{\text{esc}}^{\text{bh}} \propto M_*^{-1}$ and has a value of $f_{\text{esc}}^{\text{bh}} \sim 40\%$ (5%) for $M_* \sim 10^{9.5}$ (10^{11}) M_\odot .

We show the cumulative AGN contribution to reionization for both of these $f_{\text{esc}}^{\text{bh}}$ models in Fig. 5. Qualitatively, our results remain unchanged in that even in the “Merloni” $f_{\text{esc}}^{\text{bh}}$ scenario, AGN contribute less than a third ($\sim 30\%$) of the photons to reionization by the end of the process at $z_{\text{reio}} \sim 6.5$; this is slightly larger than the 22% photons provided by AGN in the *fiducial* model by $z_{\text{reio}} = 5.9$. A key difference between these models is that as a result of $f_{\text{esc}}^{\text{bh}}$ increasing with M_* , in the “Merloni” model black holes in high-mass galaxies ($M_* \gtrsim 10^9 M_\odot$) always make up the dominant AGN contribution. This model also shows a steeper slope of AGN contribution to reionization with decreasing redshift as increasingly massive black holes assemble and start contributing to reionization through a larger escaping output of ionizing photons.

4. Conclusions and discussion

With its sensitivity in the rest-frame optical, the JWST has yielded an unprecedented sample of black holes in the first billion years, comprising both intrinsically faint and reddened sources. Together, these objects could contribute as much as 15% to the observed (i.e. dust attenuated) UV LF at intermediate luminosities ($M_{UV} \sim -18$ to -21) at $z \sim 5$. We use the DELPHI semi-analytic model (Dayal et al. 2019), tuned to the latest galaxy and AGN observables at $z \sim 5 - 9$, to revisit the black hole contribution to reionization in light of these results. We include heavy seeding mechanisms and allow high accretion rates to reproduce the observables for AGN at $z \sim 5 - 7$. In addition to a detailed model for the dust enrichment of early galaxies (introduced in Dayal et al. 2020), we include a phenomenological model for the dust attenuation of black holes. Finally, we use low-redshift analogues of Lyman continuum emitters to link the escape fraction of ionizing photons from star formation (f_{esc}^{sf}) to the dust-attenuated UV magnitude; we assume the escape fraction of ionizing photons from black holes (f_{esc}^{bh}) to be the same as the escape fraction of UV photons in the *fiducial* model. With this model, which matches the key reionization constraints (the electron scattering optical depth and the emissivity) and includes roughly 0.5 dex of scatter on all free parameters, our key findings are:

- While star forming galaxies dominate the faint-to-intermediate end of the UV LF ($M_{UV} \gtrsim -21$), AGN determine the behaviour at the bright end at $z \sim 5$. However, the importance of AGN decreases with increasing redshift such that they are sub-dominant at all magnitudes by $z \sim 10$.
- The intrinsic production rate of ionizing photons from star formation scale roughly linearly with M_* as $\dot{n}_{int}^{sf} = 0.9M_* + \delta$ where $\delta = (45.9, 46.6)$ at $z \sim (5, 10)$. The production rate of ionizing photons from AGN is mass- and redshift-dependent: while AGN dominate over star-formation for $M_* \sim 10^{9.2-11.4} M_\odot$ galaxies at $z \sim 5$, their contribution becomes sub-dominant at all stellar masses by $z \sim 10$.
- The value of f_{esc}^{sf} decreases with M_* as galaxies become more dust enriched. For example, at $z \sim 5$, f_{esc}^{sf} drops from about 16% to $< 1\%$ as M_* increases from 10^7 to $10^{12} M_\odot$. On the other hand $f_{esc}^{bh} > 80\%$ for $m_* \lesssim 10^{8.5} M_\odot$ and shows a steep drop with increasing masses at all $z \sim 5 - 10$.
- In the *fiducial* model, reionization reaches its mid-point at $z \sim 6.9$ and is over by $z \sim 5.9$. Low-mass ($M_* \lesssim 10^9 M_\odot$) star forming galaxies are the key drivers of the reionization process, providing $> 80\%$ of ionizing photons at any redshift between $z \sim 7.1 - 20$; higher mass galaxies provide less than 5% of ionizing photons at any redshift.
- As an increasing number of black holes start accreting efficiently with decreasing redshift, the AGN contribution rises from about 26% at the mid-point of reionization ($z \sim 7$) to dominating the instantaneous budget ($\sim 66\%$) by the end-stages at $z \sim 5.9$. This is mostly driven by AGN in high-mass halos ($M_* \gtrsim 10^9 M_\odot$).
- Despite their high numbers, high accretion rates and higher escape fractions, AGN only contribute as much as star forming galaxies in terms of the ionizing budget by $z \sim 6.2$ when reionization is already in its end stages.
- Overall, low-mass star forming galaxies ($M_* \lesssim 10^9 M_\odot$) provide $\sim 77\%$ of the cumulative photon budget; star formation in higher mass halos play a negligible role, providing $< 3\%$ of the total reionization photon budget. AGN provide about 23% of the total reionization budget, mostly driven by AGN in high-mass halos ($M_* \gtrsim 10^9 M_\odot$) with AGN in low-mass halos providing the final $\sim 6.5\%$ of reionization photons.

- A model with $f_{esc}^{bh} = 1$ can be ruled out since it severely exceeds the observed emissivity constraints at $z \lesssim 6$.
- Finally we find that, provided $f_{esc}^{bh} < 1$, even contrasting models of f_{esc}^{bh} where $f_{esc}^{bh} \propto M_*$ or $f_{esc}^{bh} \propto M_*^{-1}$ do not affect our results significantly, with AGN providing less than a third of the total photon budget needed for reionization.

Our result of low-mass galaxies dominating the reionization process, with AGN affecting it in its end-stages are in good agreement with a number of previous works (Robertson et al. 2015; Atek et al. 2024; Chardin et al. 2017; Onoue et al. 2017; Dayal et al. 2020; Trebitsch et al. 2023). A key caveat, however, persists with regards to the exact nature and number densities of faint AGN. The origin of the UV emission is unclear in the case of the LRDs, and in Fig. 1 their observed UV luminosity is attributed solely to black hole accretion. However, for faint AGN, the UV luminosity could trace both the star forming and AGN components (Maiolino private communication). Detailed spectroscopic analyses will be crucial in shedding light on the nature and numbers of such objects. Additionally, combining the results from multiple surveys will be crucial in getting a handle on the cosmic variance associated with their number densities. We also caution that we have used an extremely simple geometrical model for the escape fraction model used for both star forming galaxies and AGN. While we assume spherical symmetry, the complex ISM might have a number of sight-lines that could allow a lower/higher escape fraction of both UV photons and ionizing radiation; this line-of-sight escape remains a key outstanding issue, solving which would benefit tremendously from spectroscopy of such objects.

Over the next decade, we look towards cross-correlations of spectroscopically confirmed galaxies/AGN and tomographic 21cm data from (e.g.) the SKA. These will be crucial to shed light on the progress and key sources of reionization through the distribution and redshift evolution of ionized bubble sizes and their clustering (e.g. Hutter et al. 2019).

Acknowledgements. PD acknowledge support from the NWO grant 016.VIDI.189.162 (“ODIN”) and warmly thanks the European Commission’s and University of Groningen’s CO-FUND Rosalind Franklin program. J.E.G. acknowledges support from NSF/AAG grant 1007094, and also support from NSF/AAG grant 1007052. VK acknowledges funding from the Dutch Research Council (NWO) through the award of the Vici Grant VI.C.212.036. The research of CCW is supported by NOIRLab, which is managed by the Association of Universities for Research in Astronomy (AURA) under a cooperative agreement with the National Science Foundation. AZ acknowledges support by Grant No. 2020750 from the United States-Israel Binational Science Foundation (BSF) and Grant No. 2109066 from the United States National Science Foundation (NSF); by the Ministry of Science & Technology, Israel; and by the Israel Science Foundation Grant No. 864/23. HA and IC acknowledge support from CNES, focused on the JWST mission, and the Programme National Cosmology and Galaxies (PNCG) of CNRS/INSU with INP and IN2P3, co-funded by CEA and CNES. KG and TN acknowledge support from Australian Research Council Laureate Fellowship FL180100060. This work has received funding from the Swiss State Secretariat for Education, Research and Innovation (SERI) under contract number MB22.00072, as well as from the Swiss National Science Foundation (SNSF) through project grant 200020_207349. The Cosmic Dawn Center (DAWN) is funded by the Danish National Research Foundation under grant DNRF140. We also thank the referee for their insightful comments.

References

- Akiyama, M., He, W., Ikeda, H., et al. 2018, PASJ, 70, S34
- Alexander, T. & Natarajan, P. 2014, Science, 345, 1330
- Amaro-Seoane, P., Andrews, J., Arca Sedda, M., et al. 2023, Living Reviews in Relativity, 26, 2
- Atek, H., Labbé, I., Furtak, L. J., et al. 2024, Nature, 626, 975
- Becker, G. D. & Bolton, J. S. 2013, MNRAS, 436, 1023
- Becker, G. D., D’Aloisio, A., Christenson, H. M., et al. 2021, MNRAS, 508, 1853

- Belczynski, K., Kalogera, V., & Bulik, T. 2002, *ApJ*, 572, 407
- B  thermin, M., Fudamoto, Y., Ginolfi, M., et al. 2020, *A&A*, 643, A2
- Bogd  n,   ., Goulding, A. D., Natarajan, P., et al. 2024, *Nature Astronomy*, 8, 126
- Bosman, S. E. I., Davies, F. B., Becker, G. D., et al. 2022, *MNRAS*, 514, 55
- Boutsia, K., Grazian, A., Giallongo, E., Fiore, F., & Civano, F. 2018, *ApJ*, 869, 20
- Bouwens, R. J., Illingworth, G. D., Oesch, P. A., & et. al. 2014, *ApJ*, 793, 115
- Bouwens, R. J., Oesch, P. A., Stefanon, M., et al. 2021, *AJ*, 162, 47
- Bouwens, R. J., Smit, R., Schouws, S., et al. 2022, *ApJ*, 931, 160
- Bower, R. G., Schaye, J., Frenk, C. S., et al. 2017, *MNRAS*, 465, 32
- Bowler, R. A. A., Jarvis, M. J., Dunlop, J. S., et al. 2020, *MNRAS*, 493, 2059
- Chardin, J., Puchwein, E., & Haehnelt, M. G. 2017, *MNRAS*, 465, 3429
- Chisholm, J., Saldana-Lopez, A., Flury, S., et al. 2022, *MNRAS*, 517, 5104
- Choudhury, T. R. & Dayal, P. 2019, *MNRAS*, 482, L19
- Circosta, C., Vignali, C., Gilli, R., et al. 2019, *A&A*, 623, A172
- Davies, F. B., Hennawi, J. F., Ba  ados, E., et al. 2018, *ApJ*, 864, 142
- Dayal, P. & Ferrara, A. 2018, *Phys. Rep.*, 780, 1
- Dayal, P., Ferrara, A., Sommovigo, L., et al. 2022, *MNRAS*, 512, 989
- Dayal, P., Rossi, E. M., Shiralilou, B., et al. 2019, *MNRAS*, 486, 2336
- Dayal, P., Volonteri, M., Choudhury, T. R., et al. 2020, *MNRAS*, 495, 3065
- Devecchi, B. & Volonteri, M. 2009, *ApJ*, 694, 302
- Donnan, C. T., McLeod, D. J., Dunlop, J. S., et al. 2023, *MNRAS*, 518, 6011
- Fan, X., Carilli, C. L., & Keating, B. 2006, *ARA&A*, 44, 415
- Finkelstein, S. L., Ryan, Jr., R. E., Papovich, C., & et. al. 2015, *ApJ*, 810, 71
- Flury, S. R., Jaskot, A. E., Ferguson, H. C., et al. 2022, *ApJS*, 260, 1
- Fontanot, F., Cristiani, S., Grazian, A., et al. 2023, *MNRAS*, 520, 740
- Fujimoto, S., Brammer, G. B., Watson, D., et al. 2022, *Nature*, 604, 261
- Fujimoto, S., Wang, B., Weaver, J. R., et al. 2024, *ApJ*, 977, 250
- Furtak, L. J., Labb  , I., Zitrin, A., et al. 2024, *Nature*, 628, 57
- Furtak, L. J., Zitrin, A., Plat, A., et al. 2023, *ApJ*, 952, 142
- Gaikwad, P., Haehnelt, M. G., Davies, F. B., et al. 2023, *MNRAS*, 525, 4093
- Giallongo, E., Grazian, A., Fiore, F., & et. al. 2015, *Astronomy and Astrophysics*, 578, A83
- Giallongo, E., Grazian, A., Fiore, F., et al. 2019, *ApJ*, 884, 19
- Gnedin, N. Y. 2000, *ApJ*, 542, 535
- Gnedin, N. Y., Kravtsov, A. V., & Chen, H.-W. 2008, *ApJ*, 672, 765
- Goulding, A. D., Greene, J. E., Setton, D. J., et al. 2023, *ApJ*, 955, L24
- Grazian, A., Giallongo, E., Boutsia, K., et al. 2018, *A&A*, 613, A44
- Greene, J. E., Labbe, I., Goulding, A. D., et al. 2024, *ApJ*, 964, 39
- Harikane, Y., Nakajima, K., Ouchi, M., et al. 2024, *ApJ*, 960, 56
- Harikane, Y., Ono, Y., Ouchi, M., et al. 2022, *ApJS*, 259, 20
- Harikane, Y., Ouchi, M., Oguri, M., et al. 2023a, *ApJS*, 265, 5
- Harikane, Y., Zhang, Y., Nakajima, K., et al. 2023b, *ApJ*, 959, 39
- Hutter, A., Dayal, P., Malhotra, S., et al. 2019, *BAAS*, 51, 57
- Hutter, A., Dayal, P., Yepes, G., et al. 2021, *MNRAS*, 503, 3698
- Jung, I., Finkelstein, S. L., Dickinson, M., et al. 2020, *ApJ*, 904, 144
- Kobayashi, C., Karakas, A. I., & Lugaro, M. 2020, *ApJ*, 900, 179
- Kocevski, D. D., Onoue, M., Inayoshi, K., et al. 2023, *ApJ*, 954, L4
- Kokorev, V., Caputi, K. I., Greene, J. E., et al. 2024, *ApJ*, 968, 38
- Kokorev, V., Fujimoto, S., Labbe, I., et al. 2023, *ApJ*, 957, L7
- Labb  , I., Greene, J. E., Bezanson, R., et al. 2023a, *arXiv e-prints*, arXiv:2306.07320
- Labb  , I., van Dokkum, P., Nelson, E., et al. 2023b, *Nature*, 616, 266
- Larson, R. L., Finkelstein, S. L., Kocevski, D. D., et al. 2023, *ApJ*, 953, L29
- Leigh, N. W. C., B  ker, T., Maccarone, T. J., & Perets, H. B. 2013, *MNRAS*, 429, 2997
- Leitherer, C., Schaerer, D., Goldader, J. D., et al. 1999, *ApJS*, 123, 3
- Lu, T.-Y., Goto, T., Tang, J.-J., et al. 2020, *ApJ*, 893, 69
- Madau, P. 2017, *ApJ*, 851, 50
- Madau, P., Haardt, F., & Rees, M. J. 1999, *ApJ*, 514, 648
- Maiolino, R., Scholtz, J., Curtis-Lake, E., et al. 2024a, *A&A*, 691, A145
- Maiolino, R., Scholtz, J., Wistok, J., et al. 2024b, *Nature*, 627, 59
- Matthee, J., Naidu, R. P., Brammer, G., et al. 2024, *ApJ*, 963, 129
- Mauerhofer, V. & Dayal, P. 2023, *MNRAS*, 526, 2196
- McGreer, I. D., Fan, X., Jiang, L., & Cai, Z. 2018, *AJ*, 155, 131
- McLeod, D. J., Donnan, C. T., McLure, R. J., et al. 2024, *MNRAS*, 527, 5004
- Merloni, A., Bongiorno, A., Brusa, M., et al. 2014, *MNRAS*, 437, 3550
- Mitra, S., Choudhury, T. R., & Ferrara, A. 2018, *MNRAS*, 473, 1416
- Nakane, M., Ouchi, M., Nakajima, K., et al. 2024, *ApJ*, 967, 28
- Natarajan, P., Pacucci, F., Ricarte, A., et al. 2024, *ApJ*, 960, L1
- Niida, M., Nagao, T., Ikeda, H., et al. 2020, *ApJ*, 904, 89
- Oesch, P. A., Bouwens, R. J., Illingworth, G. D., Labb  , I., & Stefanon, M. 2018, *ApJ*, 855, 105
- Oke, J. B. & Gunn, J. E. 1983, *Astrophysical Journal*, 266, 713
- Ono, Y., Ouchi, M., Harikane, Y., et al. 2018, *PASJ*, 70, S10
- Onoue, M., Kashikawa, N., Willott, C. J., et al. 2017, *ApJ*, 847, L15
- Paardekooper, J.-P., Khochfar, S., & Dalla Vecchia, C. 2015, *MNRAS*, 451, 2544
- Parsa, S., Dunlop, J. S., & McLure, R. J. 2018, *MNRAS*, 474, 2904
- Pawlik, A. H., Schaye, J., & van Scherpenzeel, E. 2009, *MNRAS*, 394, 1812
- Piana, O., Dayal, P., & Choudhury, T. R. 2022, *MNRAS*, 510, 5661
- Planck Collaboration, Aghanim, N., Akrami, Y., et al. 2020, *A&A*, 641, A6
- Rinaldi, P., Caputi, K. I., Iani, E., et al. 2023, *arXiv e-prints*, arXiv:2309.15671
- Robertson, B. E. 2022, *ARA&A*, 60, 121
- Robertson, B. E., Ellis, R. S., Furlanetto, S. R., & Dunlop, J. S. 2015, *ApJ*, 802, L19
- Rosdahl, J., Blaizot, J., Katz, H., et al. 2022, *MNRAS*, 515, 2386
- Salpeter, E. E. 1955, *ApJ*, 121, 161
- Scholtz, J., Maiolino, R., D'Eugenio, F., et al. 2023, *arXiv e-prints*, arXiv:2311.18731
- Shapiro, P. R. & Giroux, M. L. 1987, *ApJ*, 321, L107
- Sobacchi, E. & Mesinger, A. 2013, *MNRAS*, 432, 3340
- Trebtsch, M., Blaizot, J., Rosdahl, J., Devriendt, J., & Slyz, A. 2017, *MNRAS*, 470, 224
- Trebtsch, M., Dayal, P., Chisholm, J., et al. 2022, *arXiv e-prints*, arXiv:2212.06177
- Trebtsch, M., Hutter, A., Dayal, P., et al. 2023, *MNRAS*, 518, 3576
- Trebtsch, M., Volonteri, M., & Dubois, Y. 2019, *MNRAS*, 487, 819
-   bler, H., Maiolino, R., Curtis-Lake, E., et al. 2023, *A&A*, 677, A145
- Ueda, Y., Akiyama, M., Hasinger, G., Miyaji, T., & Watson, M. G. 2014, *ApJ*, 786, 104
- Yang, J., Wang, F., Fan, X., et al. 2020a, *ApJ*, 897, L14
- Yang, J., Wang, F., Fan, X., et al. 2020b, *ApJ*, 904, 26